Access Point Selection Strategies for Indoor 5G Millimeter-Wave Distributed Antenna Systems

Zhang, L., Cotton, S., Yoo, S. K., Fernandez, M. & Scanlon, W.

DOI 10.23919/EuCAP51087.2021.9411419
ISBN 978-1-7281-8845-4

Publisher: IEEE

Access Point Selection Strategies for Indoor 5G Millimeter-Wave Distributed Antenna Systems

Lei Zhang*, Simon L. Cotton*, Seong Ki Yoo†, Marta Fernández‡ and William G. Scanlon§

*Centre for Wireless Innovation, ECIT Institute, Queen's University Belfast, BT3 9DT, U.K.
†School of Computing, Electronics, and Mathematics, Coventry University, CV1 5FB, U.K.
‡Communication Engineering Department, University of the Basque Country, 48013 Bilbao, Spain.
§Tyndall National Institute, Cork T12R5CP, Ireland.
Email: {lzhang27, simon.cotton}@qub.ac.uk; ad3869@coventry.ac.uk; marta.fernandeza@ehu.eus; w.scanlon@ieee.org

***Abstract*—In this paper, we study the use of three candidate Access Point (AP) selection mechanisms for use with indoor millimetre-wave (mmWave) Distributed Antenna Systems (DASs). These are per-sample random AP selection, one-shot AP selection and per-sample optimal AP selection. To facilitate our analysis, we used a customized measurement system operating at 60 GHz, to record the signal power time series simultaneously received at 9 ceiling mounted AP locations while a mobile user imitating a voice call application. Using the time series data, the localized cross correlation coefficient (CCC) was subsequently estimated from the raw received signal strength (RSS) using the Spearman's rank-order correlation. It was found that the resultant time series of the localized CCCs was well-described by the Gaussian distribution across all of the considered measurement scenarios. Moreover, it was observed that the line-of-sight (LOS) and quasi-LOS (QLOS) paths typically led to higher CCC values with broader spreads than the non-LOS (NLOS) scenarios. To study the potential for signal enhancement by using diversity combining in mmWave DASs, we applied selection combining, equal gain combining and maximal ratio combining before investigating the AP selection mechanisms. Finally, we provide some useful insights into the influence of differing AP numbers on the diversity gain when considering the aforementioned AP selection methods.**

***Index Terms*—access point selection, channel cross correlation, channel measurement, distributed antenna system, diversity gain, millimeter wave, time series analysis.**

I. Introduction

Millimeter-wave (mmWave) technologies are emerging as strong candidates to meet the high data rate demands of fifth generation (5G) applications, such as real-time streaming of ultra-high-definition (UHD) video and delivering augmented and virtual reality [1]. This is partially driven by the abundant availability of mmWave spectrum resources in the unlicensed frequency bands that exist globally between 57–66 GHz [2]. Compared to competing microwave frequency bands, many favorable system attributes can be attained. These include smaller antenna size (related to the shorter wavelength), lower inter-cell interference (due to the higher propagation losses) and the potential for improved security (relevant to the application of beamforming technologies).

Although the use of mmWave frequencies may provide many benefits, such as those listed above, it will also equally present as many challenges. One of these relates to the increased sensitivities to blocking and shadowing caused by obstacles which reside in the local environment [3]. This is especially true for indoor dense small cell deployments. For example, in [4] it was demonstrated that for a human body intersecting the line-of-sight (LOS) path of an indoor 60 GHz point-to-point link, signal attenuations in the range of 20–40 dB can be induced. Meanwhile, in [5], the wireless link between a 60 GHz user equipment (UE) and a wall mounted access point (AP) was studied. It was observed that compared to LOS, under non-line-of-sight (NLOS) conditions, the received signal power can deteriorate by as much as 30 dB depending on the UE usage scenario.

One possible approach which can be used to mitigate signal deteriorations related to blocking and shadowing in mmWave small cell deployments is the use of a distributed antenna system (DAS) [6]. With this objective in mind, an indoor DAS system operating at 60 GHz was investigated in [7]. Different switched diversity techniques were considered to assess their effectiveness for improving the overall performance. It was found that employing switch-and-examine combining can provide up to 9.1 dB of diversity gain. Nonetheless, one of the key metrics widely used in the analysis of diversity-based systems was omitted, namely the cross correlation [8] between the signals observed at the different AP locations.

To the best of the author's knowledge, no empirically driven study of the cross correlation of the received signal strength (RSS) experienced in indoor DASs operating at 60 GHz has appeared in the open literature. To address this issue, for the first time, we present the results of a series of experiments undertaken to statistically characterize the cross correlation encountered in indoor mmWave DASs. Furthermore, we discuss and compare the performance of different linear diversity combining techniques, i.e., selection combining (SC), equal-gain combining (EGC) and maximal-ratio combining (MRC), by considering three AP selection mechanisms which will see deployment in future mmWave DASs, namely per-sample random AP selection [9], one-shot AP selection [10], and per-sample AP selection [10].

The remainder of this paper is organized as follows. The custom 60 GHz measurement system and measurement scenarios are described in Section II. Section III discusses the

statistical analysis of the cross correlation of the RSS. The localized diversity gain for different AP numbers as well as various AP selection mechanisms are subsequently presented and discussed in Section IV. Finally, the conclusions are summarized in Section V.

II. Experimental Set-Up and Scenarios

A. Experimental set-up

To imitate a practical indoor mmWave DAS, a custom 60 GHz wireless channel measurement system was developed using the HMC6000LP711E transmitter[1] (TX) and HMC6001LP711E receiver[2] (RX) modules manufactured by Analog Devices. An identical linearly-polarized antenna-in-package with $+7.5$ dBi gain featured on both units. The half power beam width (HPBW) of the antenna is $120°$. To emulate a hypothetical 60 GHz UE, the TX module was fixed to the inside of a compact acrylonitrile butadiene styrene (ABS) enclosure (80 mm $\times$ 80 mm $\times$ 20 mm) and configured to transmit a continuous wave signal centered at 60.05 GHz with an Equivalent Isotropically Radiated Power (EIRP) of $+10.9$ dBm.

The RX module was connected to a field programmable gate array (FPGA) based v1.4 Red Pitaya data acquisition platform to emulate a mmWave AP. The 50 MHz intermediate frequency (IF) signal output of the RX module was then sampled using a 14-bit, 125 Msps analog-to-digital converter (ADC) within the Red Pitaya v1.4 platform. The FPGA unit was programmed to provide custom digital signal down conversion using the embedded software defined radio (SDR). This implementation provided an effective channel sampling frequency of 96 kHz and the RSS was subsequently downsampled by applying an averaging window of 48 consecutive samples to improve the signal to noise ratio (SNR) performance, producing an effective sampling rate of 2 kHz.

B. Experimental scenarios

The measurements were conducted in an open office area (10.62 m $\times$ 12.23 m), located on the 1st floor of the ECIT Institute at Queen's University Belfast, U.K. The floor plan is shown in Figure 1. The indoor office area comprises of several metal studded dry walls with a metal tiled floor covered with polypropylene fiber, rubber backed carpet tiles, metal ceiling with mineral fiber tiles as well as recessed louvered luminaries suspended 2.70 m above the floor level. Also present are a number of metal cabinets, PCs, chairs, desks and soft partitions. During the measurements, 9 RX boards were mounted on the ceiling at the points indicated by the red circles in Figure 1. The antenna boresight of the RXs was facing downwards, i.e., towards the floor level. A test user (an adult male of height of 1.72 m and mass 75 kg) imitated making a voice call throughout the measurement process, while holding the TX at his right ear. The TX antenna was oriented such that its boresight was facing outwards and away from the user's head. It was noted that the office area was unoccupied during the measurements to ensure that any shadowing experienced in the experiments was the result of user-induced effects and signal obstruction within the test environment. Two trajectories involving the user walking along a straight line in two opposite directions were considered, namely path AB and BA, indicated using the blue line in Figure 1. The distance of path AB/BA was 9 m, while the average walking speed of the user was estimated to be 1 m/s.

[1]https://www.analog.com/media/en/technical-documentation/data-sheets/hmc6000.pdf (visited on 16/10/2020)

[2]https://www.analog.com/media/en/technical-documentation/data-sheets/hmc6001.pdf (visited on 16/10/2020)

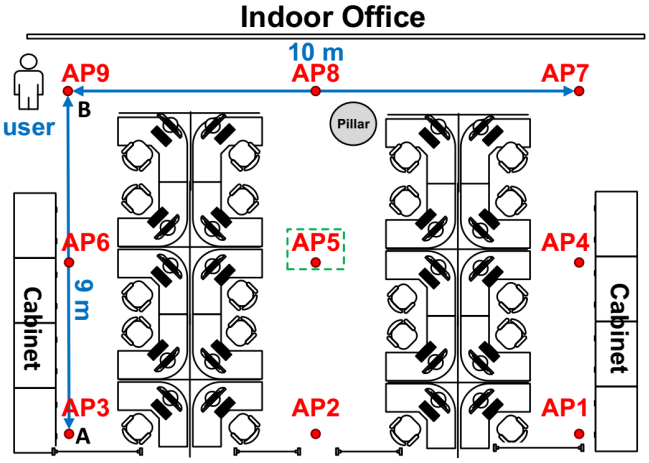

Fig. 1. Floor plan of the indoor mmWave measurement scenario environment. It is noted that AP5 (in the green dashed box) represents the target AP.

III. Channel Cross Correlation

After acquiring the raw RSS data, AP5 was selected as the target base station in the DAS since its overall mean was observed to be the highest for both paths AB and BA. Aiming to fully capture the temporal behavior of the cross correlation coefficients (CCCs) between various AP pairs, the localized CCC, introduced in [11], was adopted in this work. This was obtained by computing the CCC using a moving window of length N applied to the RSS data. An exploratory analysis of the data performed using the Kolmogorov-Smirnov (K-S) test indicated that the localized RSS observed at each of the APs was non-Gaussian in all cases. Consequently, the Spearman's rank-order correlation coefficient, was employed to calculate the localized CCCs between the RSS observed at different AP locations. The Spearman's rank-order correlation is a nonparametric measure of the monotonic relationship which exists between two variables in the ordinal form [12]. The sampled Spearman's rank-order correlation coefficient at the time instant t, denoted as $r_S(t)$, can be written as

$$r_S(t) = 1 - \frac{6\sum_{i=1}^{N}[R_{X_{ij}}(t) - R_{X_{ik}}(t)]^2}{N(N^2-1)}, \quad (j \neq k) \qquad (1)$$

where $X_{ij}(t)$ and $X_{ik}(t)$ are the corresponding RSS values of the ith sample at the time instant t, observed at the AP

TABLE I

MEAN, STANDARD DEVIATION, MINIMUM AND MAXIMUM VALUES OF THE LOCALIZED RSS SPEARMAN'S RANK-ORDER CCCS BETWEEN DIFFERENT AP LOCATIONS FOR THE PATH AB (UPPER TRIANGLE) AND THE PATH BA (LOWER TRIANGLE).

$(\mu_{r_S}, \sigma_{r_S})$ $[r_{S,\min}, r_{S,\max}]$	AP1	AP2	AP3	AP4	AP5	AP6	AP7	AP8	AP9
AP1		$(0.02, 0.18)$ $[-0.48, 0.51]$	$(-0.04, 0.16)$ $[-0.62, 0.61]$	$(0.02, 0.18)$ $[-0.66, 0.59]$	$(-0.02, 0.19)$ $[-0.66, 0.57]$	$(0.01, 0.19)$ $[-0.57, 0.62]$	$(-0.04, 0.16)$ $[-0.51, 0.41]$	$(0.01, 0.14)$ $[-0.51, 0.42]$	$(0.02, 0.15)$ $[-0.39, 0.59]$
AP2	$(-0.01, 0.12)$ $[-0.33, 0.46]$		$(0.03, 0.20)$ $[-0.53, 0.69]$	$(0.00, 0.19)$ $[-0.52, 0.77]$	$(-0.01, 0.16)$ $[-0.63, 0.40]$	$(0.01, 0.16)$ $[-0.58, 0.46]$	$(0.02, 0.11)$ $[-0.29, 0.36]$	$(-0.04, 0.13)$ $[-0.44, 0.33]$	$(0.02, 0.14)$ $[-0.33, 0.40]$
AP3	$(-0.01, 0.11)$ $[-0.31, 0.28]$	$(0.01, 0.12)$ $[-0.59, 0.39]$		$(-0.02, 0.14)$ $[-0.40, 0.41]$	$(-0.01, 0.13)$ $[-0.36, 0.41]$	$(-0.00, 0.13)$ $[-0.37, 0.43]$	$(-0.01, 0.14)$ $[-0.47, 0.38]$	$(0.01, 0.11)$ $[-0.28, 0.45]$	$(-0.00, 0.12)$ $[-0.42, 0.33]$
AP4	$(-0.00, 0.13)$ $[-0.40, 0.41]$	$(0.02, 0.12)$ $[-0.36, 0.42]$	$(-0.00, 0.12)$ $[-0.42, 0.31]$		$(0.00, 0.21)$ $[-0.66, 0.61]$	$(-0.02, 0.17)$ $[-0.55, 0.52]$	$(-0.01, 0.15)$ $[-0.47, 0.40]$	$(-0.01, 0.15)$ $[-0.47, 0.43]$	$(-0.02, 0.14)$ $[-0.49, 0.38]$
AP5	$(-0.03, 0.13)$ $[-0.43, 0.35]$	$(0.03, 0.12)$ $[-0.38, 0.38]$	$(-0.00, 0.13)$ $[-0.32, 0.43]$	$(0.01, 0.15)$ $[-0.43, 0.44]$		$(-0.01, 0.15)$ $[-0.40, 0.47]$	$(-0.01, 0.18)$ $[-0.53, 0.63]$	$(0.01, 0.16)$ $[-0.50, 0.67]$	$(-0.00, 0.14)$ $[-0.58, 0.47]$
AP6	$(0.01, 0.13)$ $[-0.32, 0.41]$	$(0.01, 0.13)$ $[-0.39, 0.36]$	$(0.00, 0.13)$ $[-0.37, 0.36]$	$(-0.01, 0.12)$ $[-0.37, 0.28]$	$(-0.01, 0.13)$ $[-0.36, 0.39]$		$(-0.04, 0.12)$ $[-0.40, 0.37]$	$(-0.02, 0.14)$ $[-0.34, 0.46]$	$(0.00, 0.10)$ $[-0.32, 0.28]$
AP7	$(-0.00, 0.14)$ $[-0.45, 0.46]$	$(0.02, 0.15)$ $[-0.37, 0.48]$	$(-0.02, 0.11)$ $[-0.40, 0.32]$	$(0.00, 0.14)$ $[-0.35, 0.48]$	$(-0.02, 0.15)$ $[-0.56, 0.47]$	$(-0.01, 0.15)$ $[-0.39, 0.40]$		$(0.02, 0.16)$ $[-0.48, 0.48]$	$(-0.02, 0.13)$ $[-0.38, 0.40]$
AP8	$(0.02, 0.13)$ $[-0.38, 0.39]$	$(-0.01, 0.13)$ $[-0.48, 0.49]$	$(0.03, 0.13)$ $[-0.29, 0.41]$	$(0.02, 0.16)$ $[-0.37, 0.57]$	$(-0.01, 0.12)$ $[-0.47, 0.37]$	$(-0.00, 0.14)$ $[-0.45, 0.46]$	$(-0.00, 0.16)$ $[-0.53, 0.56]$		$(0.05, 0.14)$ $[-0.27, 0.71]$
AP9	$(-0.01, 0.13)$ $[-0.45, 0.38]$	$(-0.01, 0.14)$ $[-0.40, 0.43]$	$(-0.02, 0.12)$ $[-0.39, 0.36]$	$(-0.04, 0.11)$ $[-0.35, 0.22]$	$(-0.03, 0.13)$ $[-0.36, 0.32]$	$(-0.02, 0.10)$ $[-0.30, 0.24]$	$(-0.00, 0.12)$ $[-0.30, 0.34]$	$(-0.02, 0.11)$ $[-0.44, 0.33]$	

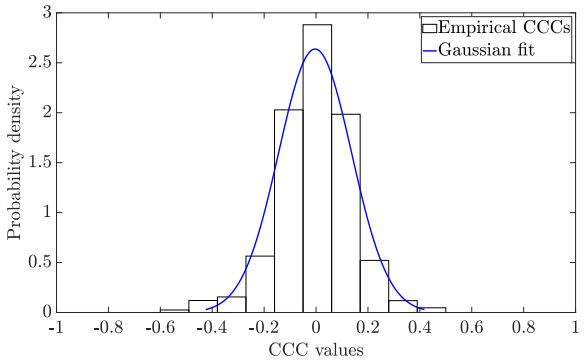

Fig. 2. The empirical PDF of $r_S(t)$ between AP5 and AP9 of the path AB along with the corresponding Gaussian distribution fit.

indexes of j and k, respectively. In (1), $R_{X_{ij}}(t)$ and $R_{X_{ik}}(t)$ represent the ranks within the RSS vectors $X_{ij}(t)$ and $X_{ik}(t)$, respectively. In this study, we considered a window size of $N = 400$, or equivalently 0.2 s.

As an example, the empirical probability density functions (PDFs) of the localized CCCs between AP5 and AP9 for the path AB are presented in Figure 2. Also included in Figure 2 is theoretical plot of the best fitting Gaussian distributions.

The mean and standard deviation of $r_S(t)$, denoted as μ_{r_S} and σ_{r_S}, of various AP pairs are given in Table I, alongside the minimum and maximum values of $r_S(t)$, denoted as $r_{S,\min}$ and $r_{S,\max}$. As shown in Table I, the range of μ_{r_S} and σ_{r_S} lies between -0.04 to 0.05 and 0.10 to 0.19, respectively. Therefore, it can be concluded that the distribution of $r_S(t)$ can be approximated by a Gaussian distribution with $\mu = 0$ and σ ranging from 0.1 to 0.2. Comparing the statistics of $r_S(t)$ between different AP pairs for both mobile paths, the μ_{r_S} and σ_{r_S} values were typically found to be higher for the path AB. A possible reason for this is that with the test user imitating making a voice call, the UE antenna boresight was facing outwards away from the user's head and towards most of the APs. As a result, the wireless links between the UE and APs were more likely to experience LOS/Quasi-LOS (QLOS) conditions. Conversely, as shown in Figure 1, the UE antenna boresight was facing towards the metal cabinets for the majority of the path BA leading to QLOS/NLOS conditions between the UE and APs. Consequently, the observed CCC values between different AP pairs are generally higher with a wider spread because of the existence of LOS/QLOS paths, while under the NLOS conditions, the increased multipath tends to assist decorrelation and hence prompts lower CCC values with a smaller spread.

IV. DIVERSITY GAIN

Three types of diversity combining technique, namely SC, EGC, and MRC, were considered to combine the signal received at the APs forming the mmWave DAS. SC is a switched combining technique that selects the AP with the highest RSS at each sample interval [13]. For an M-AP DAS which utilizes SC, the signal envelope at the output, $L_{\text{SC}}(i)$, can be written as

$$L_{\text{SC}}(i) = \max\Big(X_1(i), X_2(i), \cdots, X_M(i)\Big), \tag{2}$$

where $X_M(i)$ is the signal envelope of the ith sample at the Mth AP of the DAS.

EGC considers the case where the channel gains of different APs are equal. Following this, an equal-gain combiner simply assigns an equal weight to the signal envelope observed at each AP [13], thus the instantaneous sample output of an M-AP EGC DAS can be written as

$$L_{\text{EGC}}(i) = \frac{X_1(i) + X_2(i) + \cdots + X_M(i)}{\sqrt{M}}. \tag{3}$$

Unlike the EGC approach, MRC is performed by weighting the sampled signal of each AP with respect to its own instantaneous SNR. If we assume the noise is uncorrelated with the received signal at each AP location and the noise power is equal to unity for all the utilized APs, the instantaneous sample output of an M-AP MRC DAS can be expressed as

$$L_{\text{MRC}}(i) = \sqrt{X_1^2(i) + X_2^2(i) + \cdots + X_M^2(i)}. \quad (4)$$

An important performance metric in the context of diversity combining is diversity gain. For a macro diversity system such as a DAS, it is defined as the difference between the signal level of a target AP and that received at the output of the DAS for a given signal reliability [8]. Following the studies in [7], in this work the diversity gain was evaluated at a signal reliability of 90%. Similar to the computation of the localized CCC, we computed the localized diversity gain by applying a moving window of length N on the raw RSS data. To keep our analysis of the localized diversity gain consistent with that for the localized CCC, N was set equal to 400.

Another consideration often associated with macro diversity systems is the AP selection problem [14]. It is especially important at mmWave frequencies since a dense deployment of APs is desirable to mitigate the effects of high path loss and possible LOS blockages. It requires taking into account the additional signal processing which must be performed to combine the information received at multiple APs. This typically requires additional hardware and the burden of handling coordination between APs, which can lead to increased power consumption [15]. In the sequel, we consider three different AP selection mechanisms which have been proposed for use in future mmWave DAS deployments [9], [10]. We compare their performance in terms of the diversity gain that can be achieved when considering different numbers of APs. The AP selection mechanisms are now listed as follows:

- *Per-sample random AP selection* [9]: As the name suggests, an AP is selected randomly at each sample interval. For a fixed number of APs (M), the mean localized per-sample random AP selection diversity gain, denoted as G_{RS}, can be written as

$$G_{\text{RS}} = \frac{1}{UT} \sum_{u=1}^{U} \sum_{t=1}^{T} G(u,t), \quad (5)$$

  where U represents the number of possible AP pairs for a fixed value of M, and U can be calculated as $C_M^O = \binom{O}{M}$ (here C is the combination operator and O denotes the maximum number of APs). Besides, T represents the total sample number of the collected localized diversity gain time series, i.e., $G(u,t)$.
- *One-shot AP selection* [10]: One-shot AP selection is achieved by persisting with the connections that can achieve the maximum localized diversity gain in the first time slot. This means the UE will communicate with the exact same APs for the remaining time slots. This AP selection mechanism is more complex than the per-sample random AP selection in terms of the signal processing since a computation of C_M^O is required to select the one-shot AP pairs. The mean localized one-shot AP selection gain, denoted as G_{OS}, can be expressed as

$$G_{\text{OS}} = \frac{1}{T} \sum_{t=1}^{T} \underset{\substack{u \in [1, C_M^O] \\ t=1}}{\arg\max}\, G(u,t). \quad (6)$$

- *Per-sample optimal AP selection* [10]: This is the most complex and optimal approach. Under this scheme, optimal matching between the UE and APs is determined by choosing the AP pairs that achieve the maximum localized diversity gain in each time sample. An overall computation of $C_M^O \cdot T$ is needed in order to obtain the per-sample optimal gain performance. The mean localized per-sample optimal AP selection gain, denoted as G_{OPT}, can be written as

$$G_{\text{OPT}} = \frac{1}{T} \sum_{t=1}^{T} \underset{\substack{u \in \left[1, C_M^O\right] \\ t=i}}{\arg\max}\, G(u,t), (1 \leq i \leq T). \quad (7)$$

The effects of using increasing numbers of mmWave APs and different AP selection mechanisms on the mean localized diversity gain for the paths AB and BA are shown in Figures 3(a) to 3(c). As expected, for a fixed number of mmWave APs, the per-sample random AP selection always performed worst, while the per-sample optimal AP selection provided the best performance, e.g., when $M = 5$, for the path AB, the value of SC G_{RS} was only 8.1 dB (Figure 3(a)), while the corresponding values of the SC G_{OS} and G_{OPT} were 9.4 dB and 11.1 dB (Figure 3(b) and Figure 3(c)), respectively. This observation is the result of the per-sample random AP selection simply choosing AP pairs randomly while ignoring the instantaneous feedback contained within the RSS information. Conversely, the per-sample optimal AP selection updates the AP selection by choosing the AP pairs with the maximum localized gain per sample interval.

Most importantly, from the mean localized diversity gain plots provided in Figure 3, we can identify the optimal number of APs for each selection mechanism. For instance, for the per-sample random AP selection in Figure 3(a), it can be observed that up until $M = 6$, significant improvements in the diversity gain are achieved for all the combining schemes. Although after this point, improvements in the diversity gain were not as significant as subsequent APs were added to the system. Similar to the per-sample random AP selection, the greatest improvements in the diversity gain for the one-shot AP selection were observed for successive additions of the APs until $M = 6$ (Figure 3(b)). After this, the value of G_{OS} only marginally increased for both mobile paths, e.g., when M increased from 6 to 9, the MRC G_{OS} for the path AB only increased from 13.5 dB to 14.8 dB (i.e., a 1.3 dB improvement). Considering the extra system complexities introduced by including additional mmWave APs, using 6 APs appears to provide the optimal diversity gain performance for the one-shot AP selection mechanism. Compared to the previous two AP selection mechanisms, as shown in Figure 3(c), the G_{OPT} converged to its optimal values at a much faster rate for both paths AB and BA. This behavior is particularly noticeable for the SC and MRC schemes for $M > 4$. The reason for this is that the per-sample optimal AP selection evaluates the connections among different AP pairs during each sample interval, thus the same favorable AP pairs will always be chosen within a specific time and increasing the

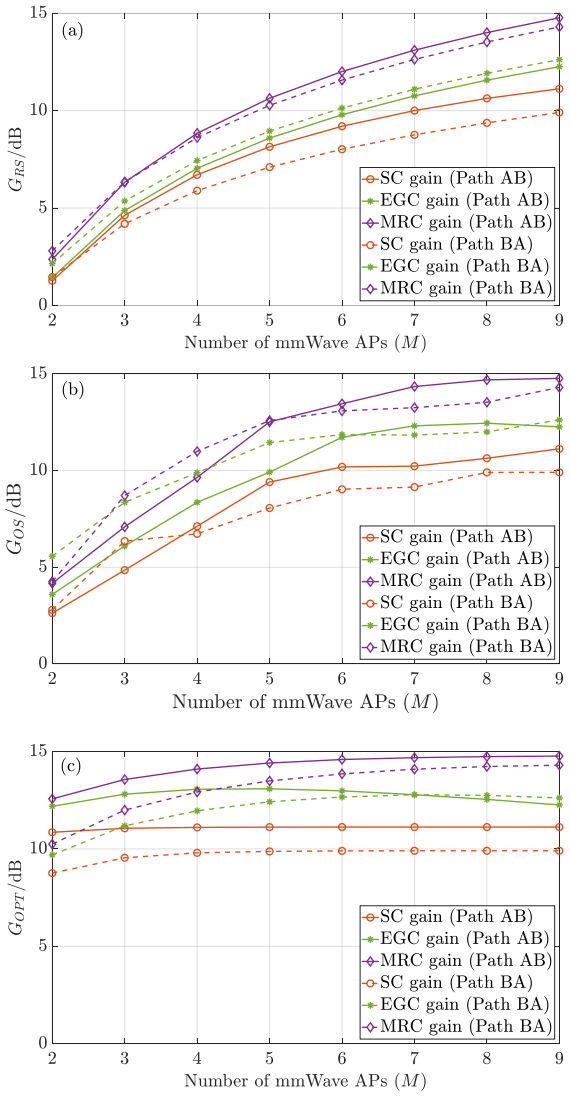

Fig. 3. The effects of using increasing numbers of mmWave APs on the mean localized diversity gain for the path AB (solid) and BA (dashed): (a) per-sample random AP selection, (b) one-shot AP selection, (c) per-sample optimal AP selection.

number of mmWave APs simply adds additional 'noisy' APs to the previously selected 'optimal' AP pairs.

V. Conclusion

Three diversity combining approaches, i.e., SC, EGC and MRC, with a UE and 9 ceiling-mounted wireless APs at 60 GHz has been statistically studied in this work. From the results, it was found out that the Gaussian distribution provided a good fit for the observed RSS CCCs over all the considered scenarios. Also, the RSS CCCs were found to be well described by a Gaussian distribution with $\mu = 0$ and σ varying from 0.1 to 0.2. Compared to the NLOS scenarios, the existence of LOS/QLOS paths produced a higher value of RSS CCCs with a broader spread. Furthermore, we considered three AP selection mechanisms for the mmWave DAS and presented the corresponding localized diversity gain performances under various AP numbers. It was discovered that the per-sample optimal AP selection showed the best diversity performance at the cost of more expensive processing, while the per-sample random AP selection performed worst but with least complexity. Most notably, based on the diversity gain results, it can be concluded that a 6-AP with one-shot AP selection and 4-AP with per-sample optimal AP selection mmWave DAS should provide satisfactory diversity performance.

Acknowledgment

This work was funded in part by the Northern Ireland Department for the Economy as part of the US-Ireland NEMOs project (USI 080).

References

[1] M. Xiao, S. Mumtaz, Y. Huang, L. Dai, Y. Li, M. Matthaiou, G. K. Karagiannidis, E. Björnson, K. Yang, I. Chih-Lin *et al.*, "Millimeter wave communications for future mobile networks," *IEEE Journal on Selected Areas in Communications*, vol. 35, no. 9, pp. 1909–1935, 2017.

[2] C. Park and T. S. Rappaport, "Short-range wireless communications for next-generation networks: UWB, 60 GHz millimeter-wave WPAN, and ZigBee," *IEEE Wireless Communications*, vol. 14, no. 4, 2007.

[3] P. Karadimas, B. Allen, and P. Smith, "Human body shadowing characterization for 60-GHz indoor short-range wireless links," *IEEE Antennas and Wireless Propagation Letters*, vol. 12, pp. 1650–1653, 2013.

[4] S. Collonge, G. Zaharia, and G. E. Zein, "Influence of the human activity on wide-band characteristics of the 60 GHz indoor radio channel," *IEEE Transactions on Wireless Communications*, vol. 3, no. 6, pp. 2396–2406, 2004.

[5] S. K. Yoo, S. L. Cotton, R. W. Heath, and Y. J. Chun, "Measurements of the 60 GHz UE to eNB channel for small cell deployments," *IEEE Wireless Communications Letters*, vol. 6, no. 2, pp. 178–181, 2017.

[6] A. A. Saleh, A. Rustako, and R. Roman, "Distributed antennas for indoor radio communications," *IEEE Transactions on Communications*, vol. 35, no. 12, pp. 1245–1251, 1987.

[7] S. K. Yoo, L. Zhang, S. L. Cotton, and H. Q. Ngo, "Distributed antenna systems used for indoor UE to access point communications at 60 GHz," in *2019 13th European Conference on Antennas and Propagation (EuCAP)*, 2019, pp. 1–5.

[8] A. M. Turkmani, A. A. Arowojolu, P. Jefford, and C. Kellett, "An experimental evaluation of the performance of two-branch space and polarization diversity schemes at 1800 MHz," *IEEE Transactions on Vehicular Technology*, vol. 44, no. 2, pp. 318–326, 1995.

[9] C. Skouroumounis, C. Psomas, and I. Krikidis, "Low-complexity base station selection scheme in mmWave cellular networks," *IEEE Transactions on Communications*, vol. 65, no. 9, pp. 4049–4064, 2017.

[10] X. Qin, X. Yuan, Z. Zhang, F. Tian, T. Hou, and W. Lou, "Joint user-AP association and resource allocation in multi-AP 60 GHz WLAN," *IEEE Transactions on Vehicular Technology*, vol. 68, no. 6, pp. 5696–5710, 2019.

[11] L. J. November, "Measurement of geometric distortion in a turbulent atmosphere," *Applied Optics*, vol. 25, no. 3, pp. 392–397, 1986.

[12] D. J. Sheskin, *Handbook of parametric and nonparametric statistical procedures*. CRC Press, 2003.

[13] D. G. Brennan, "Linear diversity combining techniques," *Proceedings of the IRE*, vol. 47, no. 6, pp. 1075–1102, 1959.

[14] M. Abusubaih, J. Gross, S. Wiethoelter, and A. Wolisz, "On access point selection in IEEE 802.11 wireless local area networks," in *Proceedings. 2006 31st IEEE Conference on Local Computer Networks*, 2006, pp. 879–886.

[15] S. Sanayei and A. Nosratinia, "Antenna selection in MIMO systems," *IEEE Communications Magazine*, vol. 42, no. 10, pp. 68–73, 2004.